ISIJ International, Vol. 56 (2016), No. 1, pp. 71–77

Effect of Fe on Carbothermic Reduction of MnO

Dong-Yuk KIM and Sung-Mo JUNG*

Graduate Institute of Ferrous Technology (GIFT), Pohang University of Science and Technology (POSTECH), Cheongam-ro 77, Pohang, 790-784 Korea.

(*Received on September 7, 2015; accepted on October 9, 2015*)

The effect of Fe addition on the carbothermic reduction of MnO has been investigated from kinetic viewpoint in the temperature ranges of 1 100–1 300°C. The addition of Fe affected the carburization rate of MnO at all the experimental temperatures. The reduction degree and carburization rate of MnO were increased with adding metallic Fe, and the most influential experiment was confirmed at the temperatures where Fe–C melt could be formed. It was confirmed that the direct carburization rate of MnO by dissolved carbon in Fe is faster than indirect carburization rate by CO gas. The carburization behavior of MnO by Fe–C melt were considerably different at 1 200°C and 1 300°C, although Fe was melted with carbon in both temperatures which are above 1 150°C. The results could be explained by not only melting rate of Fe–C but also melting point of (Mn,Fe)-carbide.

KEY WORDS: Fe addition; manganese iron carbide; carburization rate; melting rate; Fe–C melt; direct carburization.

1. Introduction

Most of ferromanganese alloys are industrially produced in EAF (Electric Submerged Arc Furnace). The smelting reduction process in EAF consumes the overall energy to increase temperature up to about 1 500°C, which corresponds to the electrical power of about 3 000 kWh/ton with 300 kg of fixed carbon.[1] In addition, nearly 40 mass% of MnO is dissolved into molten slag during the reduction of MnO, which requires more operations of high consumption of electricity and carbon for the recovery of metal yield from discarded slag containing dissolved MnO.

Reduction of manganese ore in the solid state was expected to be the alternative method due to its improved efficiency of reduction process. It was usually carried out through the carbothermic reduction of MnO as follows:[2]

$$7MnO + 10C = Mn_7C_3 + 7CO \quad \text{..... (1)}$$

Its overall reaction proceeds through intermediate gases, CO and CO_2:

$$7MnO + 13CO = Mn_7C_3 + 10CO_2 \quad \text{..... (2)}$$

$$10CO_2 + 10C = 20CO \quad \text{..... (3)}$$

The mass transfer of CO and CO_2 occurs in between oxide and graphite through gaseous reduction by Eq. (2) and carbon gasification by Eq. (3). It is well known that the gaseous atmosphere has a strong impact on the reduction of MnO, which is due to different diffusivities of CO and CO_2.[3] Since the diffusivity of CO in He was higher than that in Ar, the reduction rate of MnO in He was much faster than that in Ar. In addition, the reduction rate of MnO was even faster in H_2 than that in He even though the diffusivity of CO in H_2 is about the same as that in He. This is because H_2 could be involved directly in the reduction of MnO in terms of methane generated as intermediate species.[2]

In order for the carbothermic reduction of MnO to be completed in the solid state within allowed time, the experiments should be carried out in H_2 atmosphere accordingly. However, since the use of hydrogen for the reduction of MnO can accompany significant cost and danger in industrial production, it would be beneficial to conduct the reduction in inert gas atmosphere. Thus, it should be undertaken to find out important factors for improving the reduction rate of MnO in inert gas atmosphere.

According to Rankin and Deventer, the reduction rate of MnO by graphite was increased with adding Fe_2O_3.[4] They concluded that metallic Fe could catalyze the carbon gasification which was expected to be the rate controlling step of carbothermic reduction of MnO. However, it was not convincing at high temperatures above which the carbon gasification started to be activated significantly. Since the reduction rate of MnO was limited by the gaseous diffusion of CO and CO_2 between MnO oxide and carbon at high temperatures above 1 100°C, the effect of Fe addition on the reduction rate of MnO was unclear in the temperature range.[3,5]

The current study investigated the effect of metallic Fe on the kinetics of MnO reduction at 1 100–1 200°C. In other words, in order to identify the mechanism by Fe addition, the reduction rate of MnO by carbon was compared with varying the amount of Fe addition at different temperatures. By confirming the effect of Fe addition on the carbothermic reduciotn of MnO, the current work would contribute to the production efficiency of ferromanganese alloys.

* Corresponding author: E-mail: smjung@postech.ac.kr
DOI: http://dx.doi.org/10.2355/isijinternational.ISIJINT-2015-507

© 2016 ISIJ

2. Experimental

Homogeneous mixture of the reagent-grade chemical of MnO (63–250 μm and 99% purity) and synthetic graphite powder (5 μm and 99.7% purity) was prepared with the amount of stoichiometric molar ratio for Mn_7C_3 based on Eq. (1). The added amount of reagent-grade metallic Fe (150 μm and 99.9% purity) to the mixture of MnO and graphite was determined by the calculation according to the following reaction:

$$xMnO + yFe + \left\{\frac{10x+3y}{7}\right\}C = \frac{(x+y)}{7}(Mn,Fe)_7C_3 + xCO \quad \text{..... (4)}$$

The cylindrical tablets of 10 mm diameter were formed by pressing about 1.0 g (±0.01 g) of the mixture at 40 MPa into a cylindrical mold. The formed pellets are stored in a desiccator under 0.02 MPa before use to ensure they were dry prior to experiments.

High temperature thermogravimetric analysis (TGA) (RUBOTHERM, Germany) was employed to reduce MnO by measuring the weight change with an accuracy of 0.01 mg. An alumina crucible (12.5 mm ID and 10 mm Height) containing about 1.0 g of pellet was suspended by Pt wire, and was then placed into the isothermal zone of the furnace. High purity of Ar was blown at a flow rate of 250 mL/min by mass flow controller (MFC). The product gases were analyzed by quadrupole mass spectrometry (QMS) during the reduction in Ar gas as shown in **Fig. 1**. After completing the reduction, the sample was rapidly quenched with Ar blowing.

The reduction degree of the samples was calculated by the mass balance of oxygen in between MnO and the product gases (CO and CO_2) with an accuracy of 5 ppm obtained from QMS. Based on the Ar gas at a flow rate of 250 mL/min, the vol% of CO and CO_2 were converted into the flow rates of CO and CO_2 according to the following equation:

$$Q_i = \left(\frac{V_i}{V_{Ar}}\right) \times Q_{Ar} \quad \text{..... (5)}$$

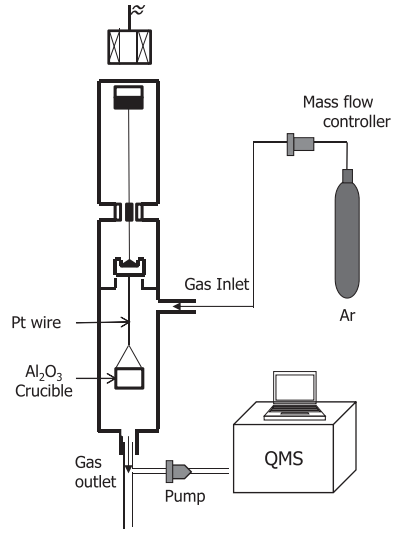

Fig. 1. Schematic illustration of experimental arrangement.

where Q_i represent the flow rates of CO and CO_2, and V_i indicates vol% of CO and CO_2. The oxygen amount contained in CO and CO_2 gases was calculated from the integration of flow rates of CO and CO_2 during the reduction as follows:

$$\text{Total flow of CO(mL)} = \sum Q_{CO} \times \text{time(min)} \quad \text{..... (6)}$$

$$\text{Total flow of } CO_2\text{(mL)} = \sum Q_{CO_2} \times \text{time(min)} \quad \text{..... (7)}$$

$$\text{Oxygen in CO(g)} = \text{Total flow of CO(mL)} \times \frac{28\ \text{g}\cdot\text{mol}^{-1}\ \text{CO}}{24\,510\ \text{mL}\cdot\text{mol}^{-1}} \times \frac{16\ \text{g}\cdot\text{mol}^{-1}\ \text{O}}{28\ \text{g}\cdot\text{mol}^{-1}\ \text{CO}} \quad \text{..... (8)}$$

$$\text{Oxygen in } CO_2\text{(g)} = \text{Total flow of } CO_2\text{(mL)} \times \frac{44\ \text{g}\cdot\text{mol}^{-1}\ CO_2}{24\,510\ \text{mL}\cdot\text{mol}^{-1}} \times \frac{2\times16\ \text{g}\cdot\text{mol}^{-1}\ \text{O}}{44\ \text{g}\cdot\text{mol}^{-1}\ CO_2} \quad \text{..... (9)}$$

Therefore, the reduction degree was finally evaluated by the following equation:

$$\text{Reduction degree (\%)} = \frac{\text{Oxygen in CO} + \text{Oxygen in } CO_2}{\text{Initial oxygen content in MnO}} \times 100 \quad \text{..... (10)}$$

About 50 mg of sample consisting of MnO, Fe and graphite was prepared as shown in **Fig. 2** to conduct the experiment by a confocal laser scanning microscope (CLSM) equipped with an image furnace of which the temperature was raised at the rate of 200°C/min in pure Ar atmosphere. In the experiments, the carburization of MnO related to the formation and melting of Fe–C alloys was observed at high temperatures.

The reduced sample was analyzed by X-ray diffraction (XRD) and Field Emission-Electron Probe Micro Analyzer (FE-EPMA) for the identification of phases and morphology observation. X-ray diffraction (D8 Advance, Bruker-AXS GmbH) using a Cu-Kα X-ray source was done by scanning from 20 to 80 degree at 2s/step with a step size of 0.02 degree. The voltage was 40 kV with a current of 40 mA. The cross-section of the sample was mirror-polished with a 1 μm diamond suspension prior to the observation of sample morphology employing FE-EPMA (JEOL JXA-8530F) operated at 15 kV and a 50 nA beam current.

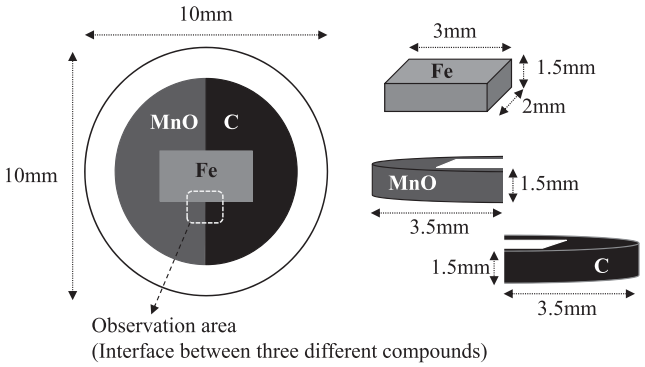

Fig. 2. Pellet assembly of MnO, Fe and C for confocal laser scanning microscope.

© 2016 ISIJ

3. Results and Discussion

3.1. Carbothermic Reduction Rate of MnO with Adding Fe at 1 100°C and 1 300°C

As shown in **Fig. 3**, the reduction experiments of MnO at 1 100°C and 1 300°C were carried out with adding Fe to compare the effect of Fe on carbothermic reduction of MnO with reference to that at 1 150°C where Fe could form melt with carbon. The degree and rate of carbothermic reduction of MnO was increased with increasing the amount of Fe addition at both temperatures. However, the effect of Fe addition was not significant at 1 100°C compared with that at 1 300°C. Metallic Fe was expected to catalyze the carbon gasification at 1 100°C,[6] but the increase in its rate was limited by the carburization of Fe in the solid state in an Ar atmosphere. As is observed in the morphology of (a) MnO reduction without Fe and (b) MnO reduction with 25 mass% Fe in **Fig. 4**, the clear difference was not identified. Numerous pores in MnO blocks were estimated to be the evidence for the gaseous reduction by CO according to Eq. (2), which could be confirmed by EPMA area mapping analyses shown in Fig. 4(a). It showed that the apparent reduced area corresponds to pores in MnO blocks identified by overlapped concentration of Mn (yellow), O (green), and C (blue). In the EPMA area mapping of MnO reduction with 25 mass% Fe at 1 100°C in Fig. 4(b), it appeared that the particles of metallic Fe were not involved directly in MnO blocks. At 1 100°C, the carbon gasification reaction was not activated fully in a way that the rate determining step would be still carbon gasification. If the carbon gasification rate could be catalyzed by metallic Fe,[7] reduction rate would also be increased with Fe addition at 1 100°C. However, the increasing extent of reduction rate of 1 100°C with Fe addition was not huge compared to that of 1 300°C with Fe addition because direct carburization effect by Fe–C melt is higher than indirect carburization effect by Fe catalyst. Therefore, it is believed that the effect of Fe addition on the degree and rate of MnO reduction was not marked at 1 100°C unlike 1 300°C.

On the other hand, the reduction rate of MnO with carbon was increased significantly with adding Fe at 1 300°C. At this temperature, the melt formation of added Fe with carbon can directly carburize MnO. As is compared in between (a) the carburized product of MnO without Fe and (b) that with 25 mass% of Fe in **Fig. 5**, the difference in the morphology was observed evidently. The carburized product of MnO without Fe at 1 300°C was not different remarkably from that at 1 100°C as shown in Fig. 5(a), which was

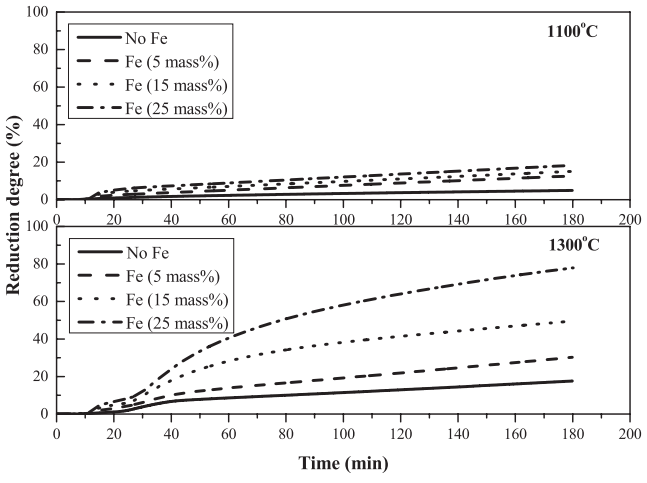

Fig. 3. Carbothermic reduction of MnO depending on Fe addition at 1 100°C and 1 300°C.

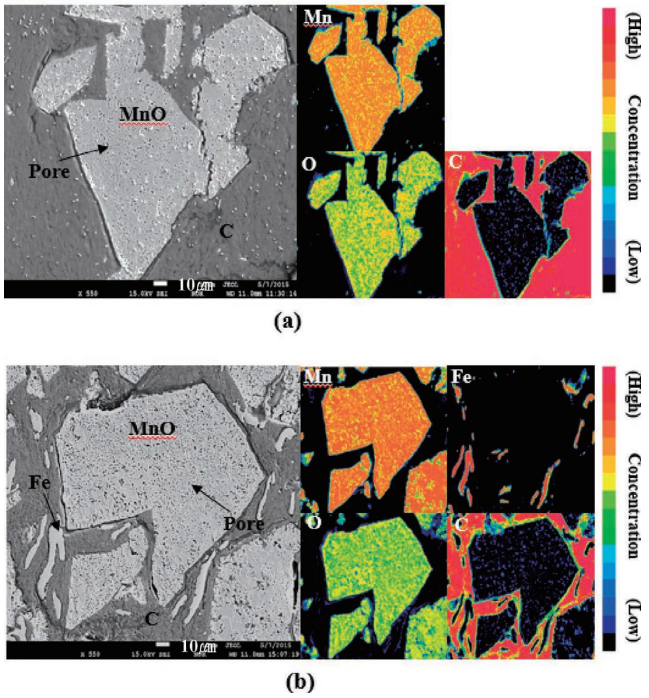

Fig. 4. EPMA area mapping of (a) the product sample of MnO carburization without Fe at 1 100°C for 180 min and (b) the product sample of MnO carburization with 25 mass% Fe at 1 100°C for 180 min.

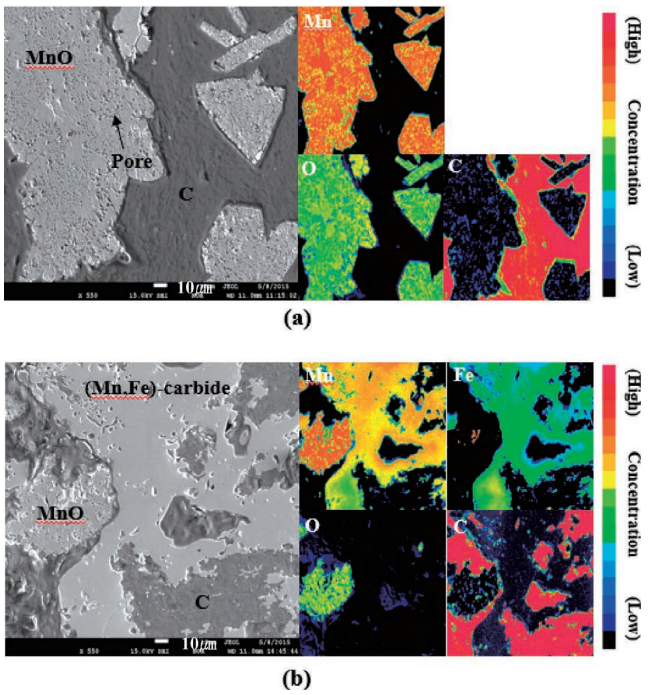

Fig. 5. EPMA area mapping of (a) the product sample of MnO carburization without Fe at 1 300°C for 180 min and (b) the product sample of MnO carburization with 25 mass% Fe at 1 300°C for 180 min.

© 2016 ISIJ

resulted from the carburization of MnO in the solid state occurring through similar process below 1 332°C, melting point of Mn–C as will be estimated later in **Fig. 12**(a). However, the carburized product of MnO with 25 mass% of Fe at 1 300°C had completely different morphology from that without Fe. Since MnO was carburized by formed melt of Fe–C, the produced (Mn,Fe)-carbide was very dense relative to MnO blocks. The (Mn,Fe)-carbide could be identified by overlapped concentration of Mn (yellow), Fe (green), O (black) and C (blue) in EPMA area mapping as shown in Fig. 5(b). However, the concentration of carbon might not be clear in (Mn,Fe)-carbide because of high concentration of resin close to them. The overlapped region of Mn and Fe without oxygen should definitely be (Mn,Fe)-carbide since it can also be confirmed by XRD results shown in **Fig. 7**.

Direct carburization of MnO through dissolved carbon in Fe–C melt is faster than indirect carburization by CO gas, which was resulted from comparison between the increasing rate of liquid phase thickness of Fe by graphite and that of by 100 vol% of CO gas.[8–10] Thus, the effect of Fe addition on carburization of MnO at 1 300°C was much more greater than that at 1 100°C because the direct carburization by Fe–C melt could take place at 1 300°C. Furthermore, the relative ratio of CO to CO_2 was increased by direct carburization of MnO at 1 300°C where Mn_7C_3 could be formed more easily at low oxygen partial pressures in the Mn–O–C stability diagram from the thermodynamic viewpoint.[11] Therefore, the carburization rate of MnO could be increased with increasing the interfacial area between MnO and Fe–C melt at 1 300°C due to the continuous contact between them.

3.2. Effect of Temperature on Carbothermic Reduction Behavior of MnO with Adding 25 mass% of Fe

Carbothermic reduction of MnO without Fe addition was compared with those with 25 wt% Fe addition in temperature range of 1 100–1 300°C as shown in **Fig. 6**. Above all, the carburization rate of MnO was increased with increasing temperature regardless of Fe addition. This is ascribed to the increased mass transfer of intermediate gases, CO and CO_2 with increasing temperature.[5,12,13] However, the effect of temperature on carburization rate of MnO was not significant, since its rate in the solid state could be limited in Ar atmosphere.[14,15] In the carburization of MnO with addition of 25 mass% Fe, the temperature was more effective on its rate than that without Fe. The effect of 25 mass% Fe addition on MnO carburization at 1 100°C was similar to that of MnO carburization without Fe addition at 1 300°C in view of the degree and rate of MnO carburization. In particular, the degree and rate of MnO reduction with adding 25 mass% Fe was increased noticeably at 1 300°C.

The carburized products of MnO could be different depending on the amount of Fe addition, even if the carburization behavior of MnO seemed to be similar. It was confirmed by XRD patterns shown in Fig. 7 where the product was Mn_7C_3 in the carburization of MnO without Fe in the temperature range of 1 100–1 300°C. Mn_7C_3 is the most stable compound in Mn–C phase diagram in the current experimental conditions for MnO carburization by sufficient carbon content.[16] The decreased peak intensity of MnO and increased peak intensity of Mn_7C_3 can represent the increase of reduction degree with increasing temperature as shown in Fig. 6. In the carburization of MnO with adding 25 mass% of Fe, $(Mn,Fe)_3C$ and $(Mn,Fe)_5C_2$ were produced instead of Mn_7C_3 since the kind of carbide can be changed by substitution of Fe for Mn in the lattice of carbide.[17] In fact, it was reported that the kind of (Mn,Fe)-carbide is changed in consecutive order, $(Mn,Fe)_3C \rightarrow (Mn,Fe)_5C_2 \rightarrow (Mn,Fe)_7C_3$, as the ratio of Mn to Fe increase from Mn–Fe–C phase diagram.[18] The formation of (Mn,Fe)-carbide started with nucleation of Fe,[2] and the possibility

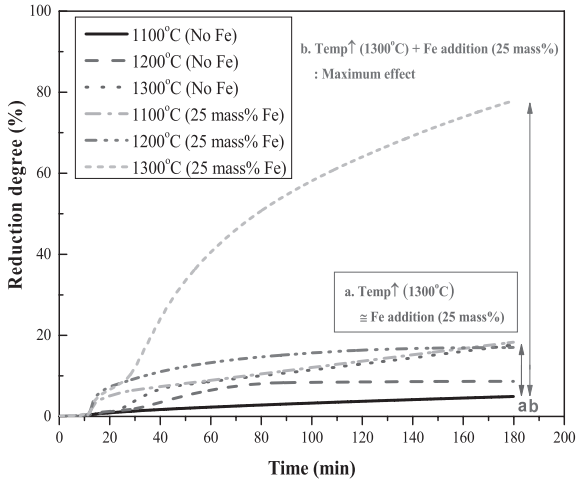

Fig. 6. Catbothermic reduction of MnO by 25 mass% Fe addition depending on temperature.

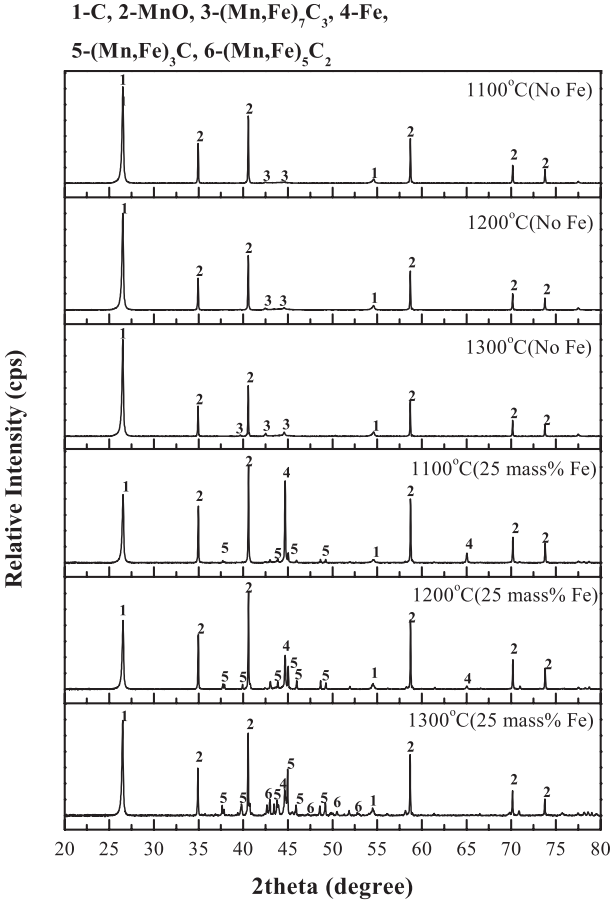

Fig. 7. XRD patterns of product from carbothermic reduction of MnO by 25 mass% Fe addition depending on temperature.

© 2016 ISIJ

of $(Mn,Fe)_3C$ formation was very high at the initial stage of carburization because the most preferential carbide is $(Mn,Fe)_3C$ thermodynamically in high ratio of Fe to Mn. Accordingly, a large amount of MnO was not carburized at 1 100°C and 1 200°C in Fig. 6 so that most of the product was $(Mn,Fe)_3C$ in the carburization of MnO with 25 mass% Fe. In the carburization of MnO with 25 mass% Fe at 1 300°C, it appeared that $(Mn,Fe)_5C_2$ was formed by XRD analysis since MnO was reduced to $(Mn,Fe)_3C$ substantially. Even if the reduction degrees in between MnO carburization without Fe at 1 300°C and that with 25 mass% Fe at 1 100°C, the products were totally different as Mn_7C_3 and $(Mn,Fe)_3C$, respectively. Therefore, it could be concluded that MnO with 25 mass% Fe at 1 100°C was more effectively carburized where the carbides of high metal yield could be produced for the identical carbon consumption.

3.3. Carburization of MnO with Fe–C Melt Formed at Different Temperatures

In the carburization of MnO with 25 mass% Fe, its degree and rate were markedly increased at 1 300°C compared with those at 1 200°C, even if it was possible for Fe–C melt to directly carburize MnO at both temperatures. To investigate the definite difference in the carburization process at 1 200°C and 1 300°C, the behavior of the sample assembly was observed by the confocal laser scanning microscope (CLSM). The carburization process of MnO with Fe–C melt formed by adding 25 mass% Fe at 1 200°C was shown in **Fig. 8**. Metallic Fe started to be melted with carbon at the interface between Fe and C in Figs. 8(a) and 8(b). Fe–C melt was kept in close contact with MnO at the interface while metallic Fe was carburized and melted by carbon with time as shown in Fig. 8(c). The Fe–C melt penetrated into MnO adjacent to carbon for carburizing MnO, but it was solidified as soon as carburizing MnO as shown in Fig. 8(d). The Fe–C melt could not penetrate into the interface between MnO and carbon due to the formation of $(Mn,Fe)_3C$ by the carburization of MnO with Fe–C melt. $(Mn,Fe)_3C$ cannot be melted at 1 200°C which is below its melting point as shown in Fig. 12(b). In addition, the reacting surface of MnO was limited except for the interface between MnO and C because the carburizing and melting rate of Fe with C were quite slow at 1 200°C as shown in Fig. 8(e). At the end of experiment as shown in Fig. 8(f), MnO could be carburized by $(Mn,Fe)_3C$ formed in between MnO and carbon, but the direct carburization was not performed anymore by Fe–C melt.

In the carburization of MnO with carbon containing 25 mass% Fe at 1 300°C, the consecutive carburizing reactions with Fe–C melt took place as shown in **Fig. 9**. That is, the formation of Fe–C melt at 1 300°C was initiated at the interface between Fe and carbon earlier than that at 1 200°C in Figs. 9(a) and 9(b). In Fig. 9(c), the Fe–C melt penetrated into MnO, leading to the generation of numerous bubbles which were CO gas released by the direct carburization of MnO as follows:

$$MnO + (Fe - C)melt = (Mn,Fe)_3C + CO \quad \text{..... (11)}$$

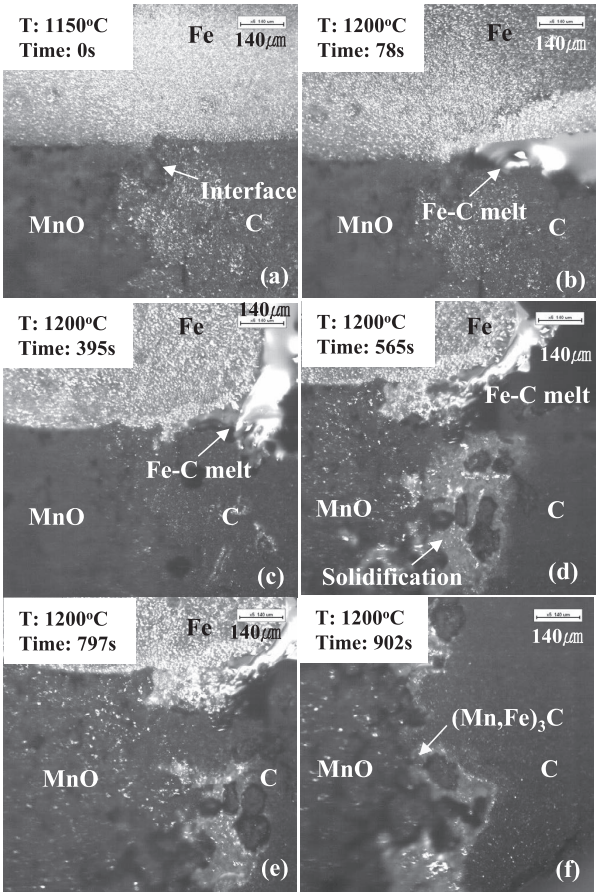

Fig. 8. Carburization process of MnO with Fe–C melting by 25 mass% Fe addition at 1 200°C.

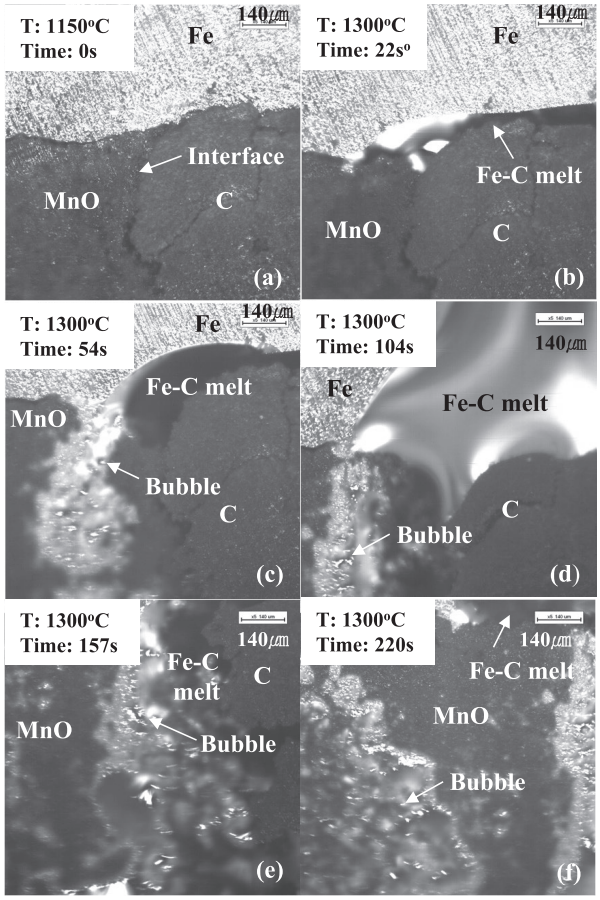

Fig. 9. Carburization process of MnO with Fe–C melting by 25 mass% Fe addition at 1 300°C.

© 2016 ISIJ

The carburizing and melting rate of Fe with carbon was so fast that it started to surround the surface of MnO for carburization gradually as shown in Fig. 9(d). The Fe–C melt continued to surround and carburize MnO without the solidification of products, $(Mn,Fe)_3C$ and $(Mn,Fe)_5C_2$, as shown in Fig. 9(e). The produced carbides can be melted at 1 300°C which is above their melting points shown in Fig. 12(b). The Fe–C melt carburized most of the MnO while actively producing numerous bubbles of CO toward the end of carburization as shown in Fig. 9(f).

In this case, heat transfer between liquid Fe–C and solid MnO could be ignored since carburization reaction of MnO is controlled considerably by carbon diffusion in Fe–C melt above 1 150°C. We simply considered the mass transfer of carbon in Fe–C melt depending on temperature. Therefore, the definite difference in the carburization rate of MnO with carbon containing 25 mass% Fe at 1 200°C and 1 300°C might be attributed to the significant difference in the carburizing and melting rate of Fe with carbon. When the melting rate of Fe–C was increased, the carburization rate of MnO could be increased at the extensive reacting surface of MnO. **Figure 10** shows the carbon concentration profile through the interface of Fe–C melt and solid Fe. Based on the mass balance of carbon, the melting rate of Fe–C melt to solid Fe could be expressed mathematically as follows:[20]

$$(C_L - C_S)\frac{dL}{dt} = D_C^L\left(\frac{\alpha C}{\alpha n}\right)_L - D_C^S\left(\frac{\alpha C}{\alpha n}\right)_S \quad \text{..... (12)}$$

where L is the length of Fe–C melt, C_L and C_S are carbon concentrations at Fe–C melt and solid Fe side of the interface, respectively, D_C^L and D_C^S are the diffusion coefficients of carbon in Fe–C melt and solid Fe, respectively, and n is normal vector of the interface. The first term in the right side means carbon flux from Fe–C melt to the interface between liquid and solid. The second term is carbon flux from the interface to the solid Fe, but it is negligible because carbon diffusivity is much smaller in solid Fe than that in Fe–C melt. In addition, the first term can be replaced by $D_C^L\frac{(C_{gr}-C_L)}{L}$ as a first approximation. That is, Eq. (12) can be simplified to Eq. (13) as follows:

$$(C_L - C_S)\frac{dL}{dt} = D_C^L\left(\frac{\alpha C}{\alpha n}\right)_L = D_C^L\frac{(C_{gr}-C_L)}{L} \quad \text{..... (13)}$$

where C_{gr} is the concentration of saturated carbon at the interface between Fe–C melt and carbon. The integration of Eq. (13) from t=0 and L=0 to t=t and L=L gives:

$$L = \sqrt{k_p t} \quad \text{..... (14)}$$

$$k_p = \frac{2D_C^L(C_{gr}-C_L)}{C_L - C_S} \quad \text{..... (15)}$$

Thus, the melting length will be changed depending on temperature since k_p can be calculated differently from the values of C_L, C_S and C_{gr} fixed by temperature in **Fig. 11**. At 1 200°C, C_L=3.9 mass%, C_S=1.7 mass%, C_{gr}=4.4 mass% and $D_C^L = 1.047\times10^{-4}$ cm^2/s of which value was resulted from Ono's calculation.[21] Then k_p at 1 200°C could be cal-

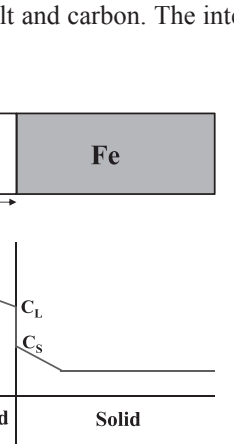

Fig. 10. Carbon concentration profile through interface of Fe–C melt and solid Fe.

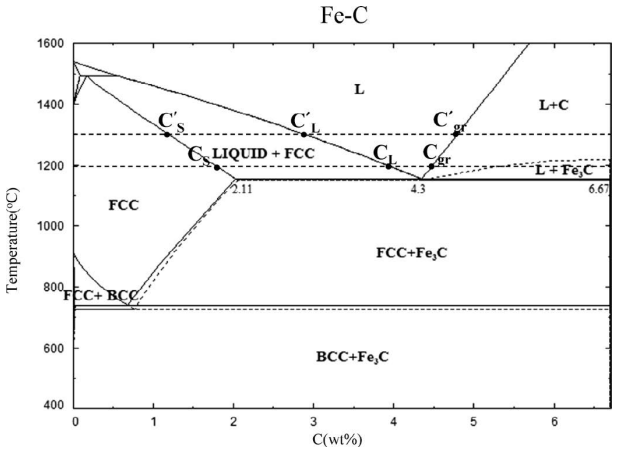

Fig. 11. Fe–C binary phase diagram.

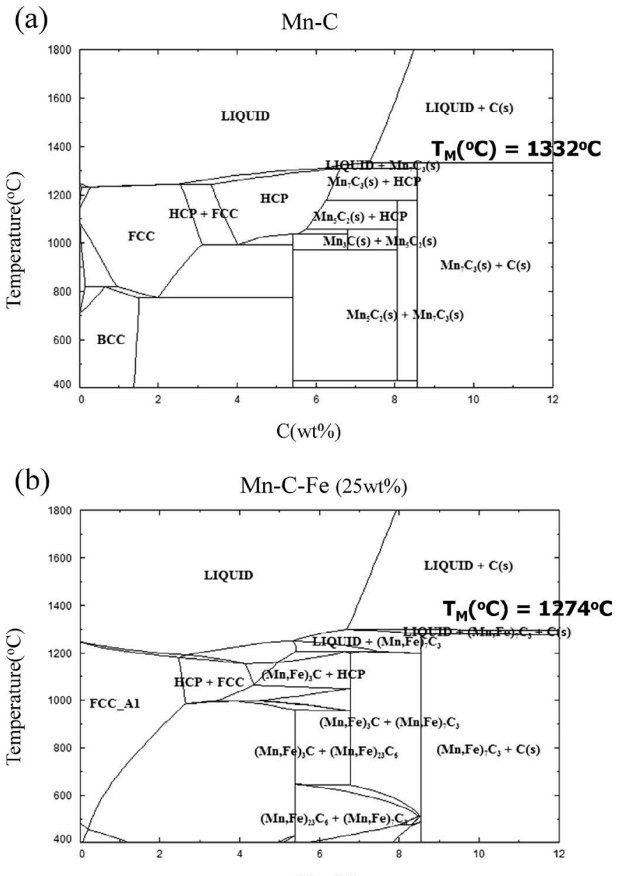

Fig. 12. (a) Mn–C phase diagram and (b) Mn–C–Fe (25 mass%) phase diagram.

© 2016 ISIJ

culated to be 4.759×10^{-5} cm^2/s. On the other hand, k_P at 1 300°C could be calculated to be 9.276×10^{-4} cm^2/s based on the values of C_L=2.9 mass%, C_S=1.2 mass%, C_{gr}=4.8 mass% and $D_C^L=1.050\times10^{-4}$ cm^2/s at 1 300°C, which were also calculated by Ono.[21] In conclusion, the melting length at 1 300°C is about 4.4 times larger than that at 1 200°C for the identical period of time in the carburization process. The direct carburization rate was limited by the interfacial area of MnO in close contact with Fe–C melt, which could be increased due to the wetting induced by the faster melting rate of Fe–C at 1 300°C rather than that at 1 200°C.

The phase diagram of Mn–C shown in Fig. 12(a) indicates that all of the manganese carbides form melts at 1 332°C regardless of carbon content, thus the carburization of MnO without Fe addition occurred in the solid state in the temperature range of 1 100°C to 1 300°C. However, the melting point of carbides could be decreased with increasing Fe addition in the phase diagram of Mn–C–Fe shown in Fig. 12(b). The temperature should be above 1 200°C at least for melting manganese iron carbide in addition to that all carbides could be melted at 1 300°C. This can also explain the difference in the carburization rate of MnO with 25 mass% Fe at 1 200°C and 1 300°C. Fe–C melt could carburize MnO, but the formed $(Mn,Fe)_3C$ at the surface of MnO was solidified at 1 200°C. Thus, the direct carburization by Fe–C melt had not great effect on the carbothermic reduction of MnO at 1 200°C since it could not contact the surface of MnO due to solidified layer of $(Mn,Fe)_3C$ shown in **Fig. 13**(a). For this reason, the carburization rate of MnO with 25 mass% Fe did not change gradually at 1 200°C in Fig. 6. On the other hand, Fe–C melt at 1 300°C could continue to carburize MnO with its constant direct carburization at the surface of MnO while $(Mn,Fe)_3C$ remains in liquid state as shown in Fig. 13(b).

This research was just carried out by pure reagent-grade MnO with graphite so that the results will be different a little bit from experimental results of manganese ores. The slag contained in ores can affect not only the melting temperature but also the carburizing rate since it can form various solid solutions with MnO and Fe depending on the chemical composition of ores. Therefore, further experiments about carbothermic reduction of manganese ores should be carried out based on the results obtained in this study.

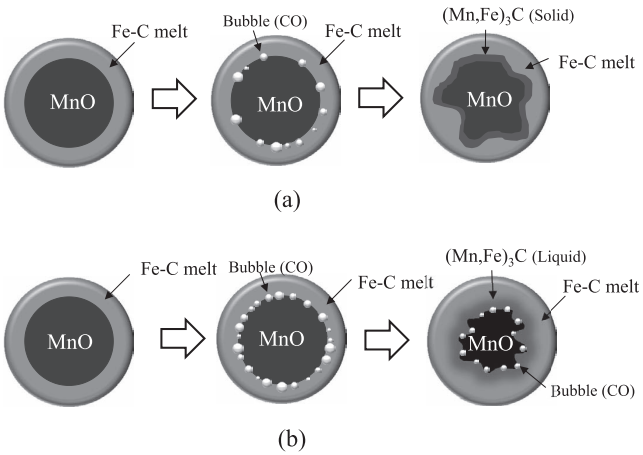

Fig. 13. Schematic mechanism for (a) carburization of MnO with Fe–C melt at 1 200°C and (b) carburization of MnO with Fe–C melt at 1 300°C.

4. Conclusions

The effect of Fe addition on carbothermic reduction of MnO was investigated in the temperature range of 1 100°C to 1 300°C. From the findings, the following conclusions were obtained:

(1) The addition of Fe significantly increased the carburization rate of MnO at 1 300°C compared with that at 1 100°C because the direct carburization of MnO by Fe–C melt could be available at 1 300°C. The metallic Fe in the solid state at 1 100°C did not affect the mass transfer of intermediate gases, CO and CO_2, which is the rate determining step of MnO carburization.

(2) With adding 25 mass% Fe to the composite of MnO and graphite, the carburization degree and rate of MnO were increased at 1 100–1 300°C. The effect of 25 mass% Fe addition at 1 100°C was comparable with that of increasing temperature to 1 300°C without Fe addition.

(3) The melting rate of Fe–C could considerably affect the carburization of MnO where its rate was determined by the direct carburization of Fe by carbon, leading to the formation of Fe–C melt. The direct carburization rate was limited by the contact area between MnO and Fe–C melt, which could be increased by the wetting of Fe–C melt of fast melting rate.

(4) The carburization rate of MnO increased consistently at 1 300°C, while it did not change much at 1 200°C although the direct carburization by Fe–C melt were available at both temperatures. The formed $(Mn,Fe)_3C$ was solidified at the surface of MnO, so that the Fe–C melt could not penetrate into MnO at 1 200°C anymore as is different from the case at 1 300°C.

REFERENCES

1) S. E. Olsen, M. Tangstad and T. Lindstad: Production of Manganese Ferroalloys, SINTEF and Tapir Academic Press, Trondheim, Norway, (2007), 46.
2) R. Kononov, O. Ostrovski and S. Ganguly: *ISIJ Int.*, **49** (2009), 1099.
3) R. Kononov, O. Ostrovski and S. Ganguly: *Metall. Mater. Trans. B*, **39B** (2008), 662.
4) W. J. Rankin and J. S. J. Van deventer: *J. S. Afr. Inst. Min. Metall.*, **80** (1980), 239.
5) W. J. Rankin and J. R. Wynnyckyj: *Metall. Mater. Trans. B*, **28B** (1997), 307.
6) F. J. Vastola and P. Lwalker, Jr.: *J. Chim. Phys.*, **58** (1961), 20.
7) A. K. Biswas: Principles of Blast Furnace Ironmaking, SBA Pub., Calcutta, India, (1981), 70.
8) Y. Sasaki, R. Asano and K. Ishii: *ISIJ Int.*, **41** (2001), 209.
9) T. Murakami and K. Nagata: *Miner. Proc. Extrac. Metall. Rev.*, **24** (2003), 253.
10) T. Murakami: Tokyo Institute of Technology, Japan, 2002, PhD. Thesis.
11) D. Kim, H. Kim and Y. Sasaki: *ISIJ Int.*, **55** (2015), 504.
12) J. Szekely, J. W. Evans and H. Y. Sohn: Gas-Solid reaction, Academic Press, New York, (1976), 178.
13) Y. K. Rao: *Metall. Trans.*, **2** (1971), 1439.
14) R. Kononov, O. Ostrovski and S. Ganguly: *ISIJ Int.*, **49** (2009), 1107.
15) M. Yastreboff, O. Ostrovski and S. Ganguly: *ISIJ Int.*, **43** (2003), 161.
16) A. I. Zaitsev, N. E. Zaitseva, Yu. P. Alekseeva and S. F. Dunaev: *Doklady Phys. Chem.*, **395** (2004), 632.
17) V. Raghavan: *J. Phase Equilib. Diff.*, **34** (2013), 131.
18) D. Djurovic, B. Hallstedt, J. Appen and R. Dronskowski: *Calphad*, **35** (2011), 479.
19) R. Kononov, O. Ostrovski and S. Ganguly: *ISIJ Int.*, **49** (2009), 1115.
20) H. Kim, S. Lee and Y. Sasaki: *ISIJ Int.*, **50** (2010), 71.
21) Y. Ono: *Tetsu-to-Hagané*, **63** (1977), 122.

© 2016 ISIJ